applied optics

Dual-grating dielectric accelerators driven by a pulse-front-tilted laser

Y. Wei,[1,2,*] M. Ibison,[1,2] G. Xia,[1,3] J. D. A. Smith,[4] and C. P. Welsch[1,2]

[1]Cockcroft Institute, Sci-Tech Daresbury, Warrington WA4 4AD, UK
[2]School of Physical Sciences, University of Liverpool, Liverpool L69 3BX, UK
[3]School of Physics and Astronomy, University of Manchester, Manchester M13 9PL, UK
[4]Tech-X UK Ltd, Sci-Tech Daresbury, Warrington WA4 4AD, UK
*Corresponding author: yelong.wei@cockcroft.ac.uk

Received 6 July 2017; revised 22 August 2017; accepted 13 September 2017; posted 13 September 2017 (Doc. ID 301819); published 9 October 2017

This paper investigates numerically dual-grating dielectric laser-driven accelerators driven by a pulse-front-tilted (PFT) laser, which extends the interaction length and boosts the electrons' energy gain. The optical system necessary to generate PFT laser beams with an ultrashort pulse duration of 100 fs is also studied in detail. Through two-dimensional particle-in-cell simulations, we show that such a PFT laser effectively increases the energy gain by (91 ± 25) % compared to that of a normally incident laser with a waist radius of 50 μm for a 100-period dual-grating structure.

OCIS codes: (230.1950) Diffraction gratings; (350.4238) Nanophotonics and photonic crystals; (350.4990) Particles; (350.5500) Propagation.
https://doi.org/10.1364/AO.56.008201

1. INTRODUCTION

Dielectric laser-driven accelerators (DLAs) utilizing the large electric fields from commercial laser systems to accelerate particles with high gradients of the order of gigavolts/meter (GV/m), have the potential to realize for the first time an on-chip particle accelerator. Grating-based structures as proposed by Plettner *et al.* [1] are among the candidates for DLAs. They can be mass-produced using available nanofabrication techniques due to their simpler structural geometry compared to other types of DLAs [2–4]. This offers for the future a far less expensive way to build high-performance particle accelerators of much smaller size than conventional ones. To date, grating-based structures have been demonstrated experimentally at accelerating gradients of up to 300 MV/m [5] and 690 MV/m [6] for relativistic electron acceleration, and at gradients of 25 MV/m [7], 220 MV/m [8], and 370 MV/m [9] for nonrelativistic electron acceleration.

Many geometric optimizations [10–13] have been carried out to maximize the accelerating gradient, resulting in the large electron energy gain for grating-based DLAs. However, previous DLA studies were performed with a normally incident laser beam. In this case, the increase in electron energy is limited by the short interaction length between the laser pulses and the electron bunch. In this paper we explore dual-grating DLAs driven by a pulse-front-tilted (PFT) laser to extend the interaction length, resulting in a larger energy gain for the DLAs. As shown in Fig. 1, a PFT laser beam is introduced to interact with an electron bunch in a dual-grating structure. The tilt angle γ can be chosen to overlap an electron bunch synchronously with the laser pulse envelope so that the electrons gain the largest possible energy. Section 2 presents a theoretical analysis for laser-bunch interaction in dual-grating structures that are illuminated by a normal or by a PFT laser beam. A comparison of both illumination schemes is also discussed. In Section 3, the detailed optical system to generate a PFT laser beam with an ultrashort pulse duration is described from mathematical calculations. Finally, in Section 4, 2D particle-in-cell simulations are carried out by introducing a PFT laser beam into a 100-period dual-grating structure to interact with a 50-MeV electron bunch. In addition, potential applications and limitations of PFT laser illumination are discussed.

2. ANALYTICAL COMPARISON

Linearly polarized Gaussian laser pulses are introduced along the y axis to illuminate the dual-grating structure while the electrons are traveling in the channel center along the z axis, which is the normal scheme for DLAs, as shown in Fig. 2(a). Such a laser pulse exhibits a cycle-averaged electric field as follows:

$$E_z = E_p e^{-\left(\frac{z}{w_z}\right)^2 - 2\ln 2\left(\frac{t}{\tau}\right)^2} \cos(\omega t - k_0 y + \phi_1), \quad (1)$$

where E_p, w_z, τ, ω, k_0, and ϕ_1 represent the peak field, z-axis waist radius, full width at half-maximum (FWHM) duration,

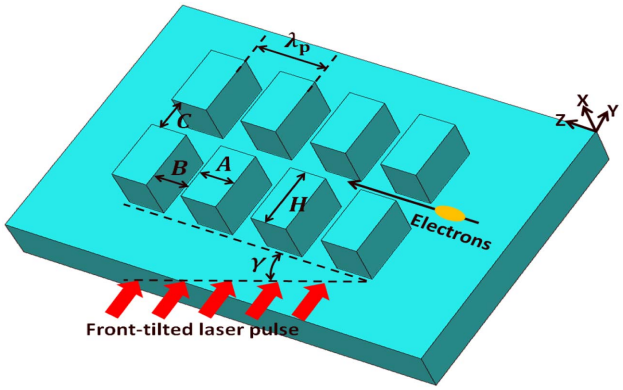

Fig. 1. Schematic of a dual-grating structure illuminated by a PFT laser beam with a tilt angle of γ. λ_p, A, B, C, and H represent grating period, pillar width, pillar trench, vacuum channel gap, and pillar height, respectively. $A + B = \lambda_p$ is selected for all simulations.

angular frequency, wave number, and phase term, respectively. In a co-moving frame, electrons move along the z axis at a speed $v = \beta c$ and experience the optical phase periodically, $z = \beta ct$; we can therefore derive the temporal electric field E_t, which electrons experience in the channel [14],

$$E_t = G_p e^{-\left(\frac{z}{w_{int}}\right)^2} \cos(\omega t - k_z z + \phi_2), \tag{2}$$

where $w_{int} = \left(\frac{1}{w_z^2} + \frac{2\ln 2}{(\beta c\tau)^2}\right)^{-0.5}$ is the characteristic interaction length, G_p is the peak accelerating gradient related to E_p, k_z is the longitudinal wave number with $k_z = k_0/\beta$, $\beta = v/c$ for electron velocity v, and ϕ_2 is a phase term. If we then assume that the electrons experience the optimum accelerating phase, we obtain the energy gain,

$$\Delta E = \int_{z_1}^{z_2} qG_p e^{-\left(\frac{z}{w_{int}}\right)^2} dz = \int_{-0.5LZ}^{0.5LZ} qG_p e^{-\left(\frac{z}{w_{int}}\right)^2} dz, \tag{3}$$

where q is the charge of a single electron, $z_1 = -0.5LZ$ and $z_2 = 0.5LZ$ are the positions along the z axis, $z = 0$ is the longitudinal center of the dual-grating structure, and LZ is the longitudinal length of a multi-period dual-grating structure. When $LZ \gg w_{int}$, the energy gain is derived as

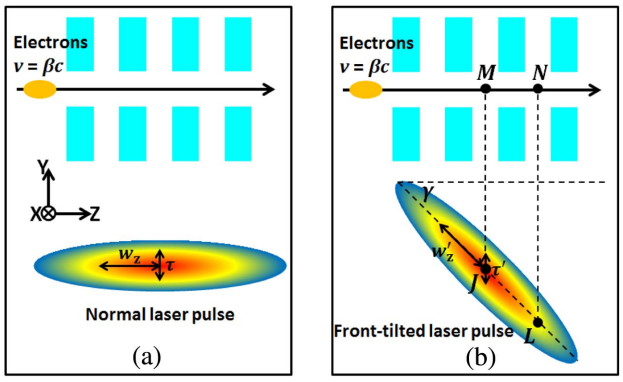

Fig. 2. Dual-grating structures are illuminated by (a) a normally incident laser pulse and (b) a front-tilted laser pulse.

$$\Delta E_m = qG_p\sqrt{\pi}\, w_{int}. \tag{4}$$

It should be noted that here the characteristic interaction length w_{int} is not the realistic interaction length $\sqrt{\pi}w_{int}$ for our analysis in this paper. In the following, what we call "interaction length" is the *characteristic* interaction length. Equation (3) indicates that a longer laser FWHM duration τ and waist radius w_z increase the interaction length w_{int}, resulting in a larger energy gain for the normal scheme. The analytically computed interaction lengths for relativistic electrons with $\beta \approx 1.0$ are illustrated in Fig. 3. It can be seen that the interaction length gradually reaches saturation with increasing waist radius for variable FWHM durations. In addition, the waist radius does not change the interaction length significantly for a 100-fs pulsed laser. Using normally incident laser illumination, Stanford Linear Accelerator Center (SLAC) has demonstrated a maximum energy gain of 24 keV over a short interaction length of 16.3 μm for a <100 fs pulsed laser [6]. In this demonstration, the interaction length was limited mainly by the short laser FWHM duration.

In the other scheme for DLAs studied here, a front-tilted laser pulse is used to illuminate the dual-grating structure, as shown in Fig. 2(b). This front-tilted laser pulse overlaps the accelerating electric field efficiently with the electron beam to extend the interaction length, thereby boosting the energy gain for the same laser parameters and grating geometries. For a sufficiently short electron bunch with velocity $\beta = v/c$ traveling from point M to N in one grating period, as seen in Fig. 2(b), the velocity of the electrons can be assumed to stay constant, i.e., $\Delta\beta/\beta \sim 0$. This is true for relativistic electrons where $\beta \approx 1.0$, as the change in velocity is practically zero. It also holds in the nonrelativistic case when the energy gain over one grating period λ_p is well below several kiloelectron volts (keV), so that the velocity of the electrons can be assumed to be constant. Figure 2(b) also shows that there is some time delay for the pulse front at points J and L to arrive at points M and N, respectively. The time delay between J and L is

$$\Delta t = \lambda_p \tan\gamma/c. \tag{5}$$

In time Δt, the electrons have traveled from M to N:

$$\lambda_p = v\Delta t, \tag{6}$$

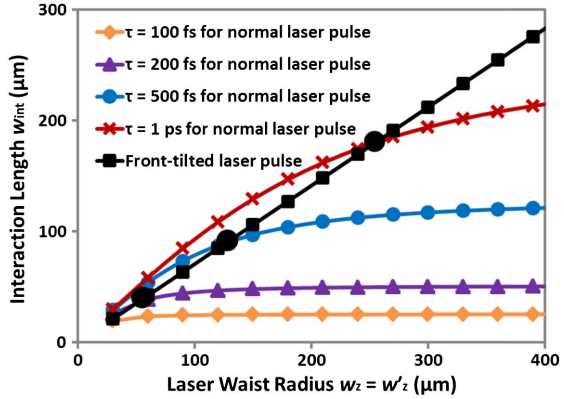

Fig. 3. Relationship between interaction length w_{int} and laser waist radius w_z with variable laser FWHM duration τ, when the electrons are relativistic with $\beta \approx 1.0$. Note that the black dots are critical waist radii at which interaction lengths are the same for both schemes.

thus

$$\beta = v/c = 1/\tan\gamma. \tag{7}$$

Equation (7) shows that the tilt angle for the pulse front is in the range of $45° \le \gamma < 90°$ and is determined by the electron injection velocity to meet the synchronicity condition.

Using the same laser frequency and wave number as for the normal DLA scheme, the electrons experience a Gaussian field along the channel center,

$$E_z' = E_p e^{-\left(\frac{z}{w_z'\cos\gamma}\right)^2 - 2\ln 2\left(\frac{t-pz}{\tau'}\right)^2}\cos(\omega t - k_0 y + \phi_1), \tag{8}$$

where w_z' is the tilted waist radius; τ' is the local pulse duration, and $p = \frac{dt}{dz}$ is the PFT factor, which is defined by the derivative of the pulse-front arrival time with respect to z; and γ is the PFT angle, as shown in Fig. 2(b). The relationship between p and γ is then given in Ref. [15] by

$$\tan\gamma = pc. \tag{9}$$

Using Eqs. (7) and (9), we can get $t - pz = 0$ when the electrons move at a speed of $v = \beta c$, So the electrons experience a Gaussian field along the channel center of

$$E_t' = G_p e^{-\left(\frac{z}{w_z'\cos\gamma}\right)^2}\cos(\omega t - k_z z + \phi_2). \tag{10}$$

It should be noted that here the distortion effect [16] is not taken into account for our analysis. When the electrons experience the optimum optical phase, the electrons' energy gain can be derived thusly:

$$\Delta E' = \int_{z_1}^{z_2} qG_p e^{-\left(\frac{z}{w_z'\cos\gamma}\right)^2}\mathrm{d}z = \int_{-0.5LZ}^{0.5LZ} qG_p e^{-\left(\frac{z}{w_z'\cos\gamma}\right)^2}\mathrm{d}z. \tag{11}$$

We can obtain the characteristic interaction length $w_{int}' = w_z'\cos\gamma$. When $LZ \gg w_z'\cos\gamma$, the energy gain is

$$\Delta E_m' = qG_p\sqrt{\pi}w_z'\cos\gamma. \tag{12}$$

Compared to Eq. (4), Eq. (12) shows that the energy gain is only related to waist radius w_z' and tilt angle γ. The interaction length is plotted as a function of waist radius in Fig. 3, where $w_z' = w_z$ and $\beta \approx 1.0$ are assumed for our calculations. For a shorter FWHM duration of $\tau \le 100$ fs, a front-tilted laser pulse generates a larger interaction length than a normally incident laser pulse. For a longer FWHM of τ>100 fs, there is a critical waist radius w_c where both schemes have the same interaction length, but when $w_z > w_c$, a front-tilted laser pulse is more efficient than a normal one.

3. OPTICAL SYSTEM REQUIRED TO GENERATE A PFT LASER

In this section, we discuss the optical system to generate the desired PFT laser. A PFT laser can be generated either by angular dispersion (AD), which causes different frequency components to propagate at different angles, or by simultaneous spatial and temporal focusing (SSTF) in the absence of AD. SSTF has been demonstrated in Ref. [17] to generate a PFT laser beam with an ultrashort pulse duration of ~100 fs at the focal region, but the waist radius is also focused to tens of micrometers (μm), thereby limiting the energy gain for DLAs. Martinez [16] has showed that the PFT laser achieved by AD gives rise to pulse broadening and changing of the tilt angle as it moves away from a diffractive grating or prism. However, these distortions can be compensated for by using an imaging system to transfer the image of a tilted pulse front on the diffraction grating into the dual-grating DLAs.

As shown in Fig. 4, our optical setup consists of a diffraction grating and a 1∶1 imaging system with a two-lens telescope. An incident laser beam experiences angular dispersion when it is propagating through a diffraction grating. This means that different spectral components of a laser pulse travel in different directions after passing the diffraction grating. As a consequence, the pulse front is tilted by an angle γ, whereas the phase fronts of the pulse are always perpendicular to the pulse propagation direction. In order to reduce the distortion, a 1∶1 imaging system with a two-lens telescope is used to re-create the same pulse front tilt, which can be introduced to illuminate a dual-grating structure to interact with the electrons.

For the diffraction grating as shown in Fig. 4, the grating equation is

$$\sin\theta_i + \sin\theta_d = \frac{\lambda_0}{g}, \tag{13}$$

where θ_i and θ_d are the incidence and diffraction angles, respectively; λ_0 is the laser wavelength; and g is the diffraction grating period. The tilt angle is also given [18] by

$$\tan\gamma = \frac{\lambda_0}{g\cos\theta_d}. \tag{14}$$

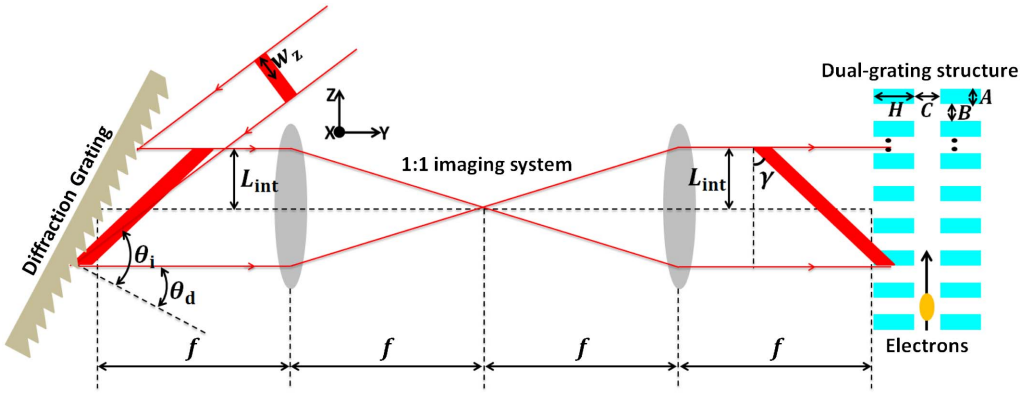

Fig. 4. Diagram of a PFT laser generated by a dedicated optical system.

In order to overlap synchronously with relativistic electrons, the PFT angle γ equals to 45°, as described in Eq. (7).

When the incidence angle θ_i is the same as the diffraction angle θ_d, the diffraction efficiency of a grating is usually maximal in the Littrow configuration. Combining with Eqs. (13) and (14), we can get $\theta_i = \theta_d = 26.6°$. When a laser wavelength of $\lambda_0 = 1.0$ μm is chosen, the diffraction grating period is $g = 1.118$ μm, corresponding to a groove density of $n_g = 894$ lines/mm for the diffraction grating. Since this is impractical, a groove density of $n_g = 900$ lines/mm is chosen as optimum for our optical system. In this case, we can get $\theta_i = 27.6°$, $\theta_d = 25.8°$.

When an incident laser pulse travels through the diffraction grating, the upper side of the pulse is diffracted by the grating earlier than the lower side of the pulse. This generates an optical path difference, which contributes to a front-tilted pulse close to the grating. Such a front-tilted pulse has the same pulse duration as the incident laser pulse. In this case, the pulse intensity and peak field remain constant. A 1:1 imaging system is then used to transfer this tilted pulse to the dual-grating structure. This imaging process does not generate any distortion for the front-tilted pulse. The imaged front-tilted pulse should be put close enough to the dual-grating structure in order to reduce the broadening effect [18]. In this paper, the pulse duration is assumed to remain constant when it is introduced into the dual-grating DLAs.

For an incident laser pulse with a waist radius w_z, the interaction length L_{int} as shown in Fig. 4 can be mathematically calculated,

$$L_{int} = \frac{\sqrt{2}\left(\left(\frac{2w_z}{\cos\theta_i}\right)^2 + (2w_z\tan\theta_i)^2 - 2\frac{2w_z}{\cos\theta_i}2w_z\tan\theta_i\cos(90°+\theta_d)\right)^{0.5}}{4}. \quad (15)$$

Equation (15) clearly shows that the interaction length L_{int} is dependent on the w_z, θ_i, and θ_d. Using such an optical system, a PFT laser beam with a peak field of E_0, a waist radius of $\sqrt{2}L_{int}$, and a local temporal duration of τ_0 can be generated. From Eq. (8), we can get the mathematical expression for the electric field of such a PFT beam,

$$E_z' = E_0 e^{-\left(\frac{z}{L_{int}}\right)^2 - 2\ln 2\left(\frac{t-pz}{\tau_0}\right)^2}\cos(\omega t - k_0 y + \phi_1). \quad (16)$$

4. PARTICLE-IN-CELL SIMULATION

In this section, the particle-in-cell code VSim [19] is used to investigate the interaction between a front-tilted laser pulse and a Gaussian electron bunch in a 100-period dual-grating structure with the following geometries: $A = B = 0.50\lambda_p$, $C = 0.50\lambda_p$, $H = \lambda_p$, $\lambda_p = 1.0$ μm, $LZ = 100.0$ μm. The electron bunch employed in our simulations has a mean energy of 50 MeV, bunch charge of 0.1 pC, root mean square (RMS) length of 9 μm, RMS radius of 10 μm, normalized emittance of 0.2 mm · mrad, and energy spread of 0.05%. It should be noted that the RMS bunch radius of 10 μm is bigger than the vacuum channel gap of 0.5 μm. Such an electron bunch can be achieved at the future Compact Linear Accelerator for Research and Applications (CLARA) [20] or the Advanced Superconducting Test Accelerator (ASTA) at Fermilab [21].

An input laser pulse with $\lambda_0 = 1.0$ μm wavelength, $\Delta P = 7$ μJ pulse energy, $\tau_0 = 100$ fs pulse duration, and $w_z = 50$ μm waist radius would generate a peak input field $E_0 = 3$ GV/m. When such a laser pulse is used for normal illumination, we find a maximum electric field of 9.10 GV/m, which is still under the damage threshold for quartz structures [1]. The calculated interaction length is $w_{int} = \left(\frac{1}{w_z^2} + \frac{2\ln 2}{(\beta c\tau_0)^2}\right)^{-0.5} = 22.7$ μm, which is much smaller than $LZ = 1.0$ μm. Using Eq. (4) with a peak accelerating gradient of $G_p = 1.0$ GV/m results in a maximum energy gain of $\Delta E_m = 40$ keV, which can be used to calculate the loaded gradient for subsequent analysis.

The same laser parameters are used for the optical system shown in Fig. 4 to generate a front-tilted pulse with an ultrashort pulse duration of $\tau_0 = 100$ fs and a tilt angle of $\gamma = 45°$. By substituting $\theta_i = 27.6°$ and $\theta_d = 25.8°$ into Eq. (15), an interaction length of $L_{int} = 51$ μm is obtained. Equation (16) is then used to mathematically model a front-tilted pulse for our 2D particle-in-cell simulation. When such a front-tilted pulse propagates through the dual-grating structure to interact with the electron bunch, the maximum energy gain is $\Delta E_m' = 75$ keV when $G_p = 1.0$ GV/m.

In our simulations, the electromagnetic fields are calculated based on the finite difference time domain (FDTD) method. The dual gratings are modelled as a 2D structure (y–z plane) because they are constant in the x direction. The mesh size is set to 10 nm(z) × 20 nm(y) so that the results are convergent. 500,000 microparticles are used for tracking in order to reduce the numerical noise in the energy spectrum. Those electrons travelling through the quartz structure suffer significant energy loss due to collisional straggling [22] in the dielectric material. Only the electrons modulated by the laser field in the vacuum channel are therefore used for our calculations. It is found that about 2% of the 50 MeV bunch is transmitted through the vacuum channel gap of 0.5 μm. Figure 5 compares the bunch energy spectrum for modulated electrons with the laser off and on. It is obvious that the energy spectrum has a double-peaked profile after laser–bunch interaction, which agrees well with the reported results [5,6,13]. Due to the numerical noise in the

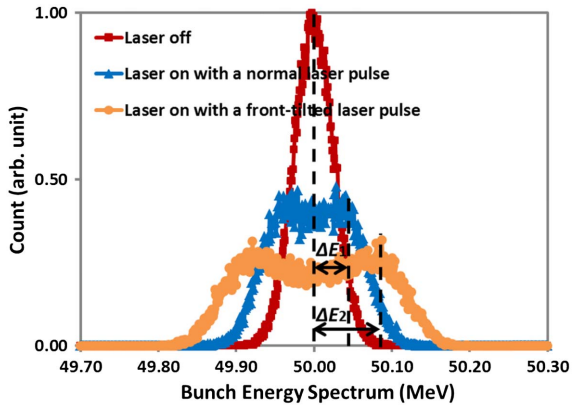

Fig. 5. Bunch energy spectrum for the cases of laser-off (red line), laser-on with a normal laser pulse (blue line), and laser-on with a front-tilted laser pulse (yellow line).

particle-tracking simulations, the calculated energy gain has an error. Figure 5 shows that the maximum energy gain is $\Delta E_1 = 43 \pm 5$ keV for normal laser illumination, whereas it is $\Delta E_2 = 82 \pm 5$ keV for PFT laser illumination. This corresponds to maximum loaded gradients of 1.08 ± 0.13 GV/m and 1.09 ± 0.07 GV/m, respectively. It is found that both schemes have similar loaded gradients, but illumination by the PFT laser generates an energy gain which is larger than the normal laser by (91 ± 25) %.

Furthermore, we also studied the effect of the tilt angle on the energy gain ΔE_2 by running particle-in-cell simulations for the same electron bunch and structure. By using Eqs. (9), (11), and (16), the energy gain with different tilt angles can be calculated analytically. Figure 6 shows the energy gain from analytical and particle-in-cell calculations with different tilt angles, and good agreement between them is found. It can be seen from Fig. 6 that the maximum energy gain $\Delta E_2 = 82 \pm 5$ keV occurs at a tilt angle $\gamma = 45°$. This strongly supports the synchronous acceleration of relativistic electrons through a PFT laser with a tilt angle of 45°, which is in good agreement with Eq. (7).

It can be seen in Eq. (15) that the interaction length L_{int} increases linearly with the waist radius w_z of the incident laser beam. By simply taking the product of the loaded gradient ~1.10 GV/m and the electrons' energy gain from Eq. (11), we can calculate the energy gain analytically. Figure 7 shows the energy gain from such analytical and particle-in-cell calculations with variable laser waist radii w_z, and very good agreement between them is found. As shown in Fig. 7, when the laser waist radius w_z increases from 50 to 500 μm, the energy gain gradually saturates. For a 100-period dual-grating, the maximum energy gain is calculated to be 110 ± 7 keV.

It should be noted that a 100-period structure with a length of $LZ = 100.0$ μm is used for our simulations due to limitations in our computing hardware. Equation (11) indicates that a larger number of periods results in a higher energy gain. Based on the same analytical calculations using the loaded gradient ~1.10 GV/m, Fig. 8 shows that the energy gain gradually saturates when the laser waist radius w_z increases from 50 to 1000 μm for the structures with 500, 1000, and 2000 periods.

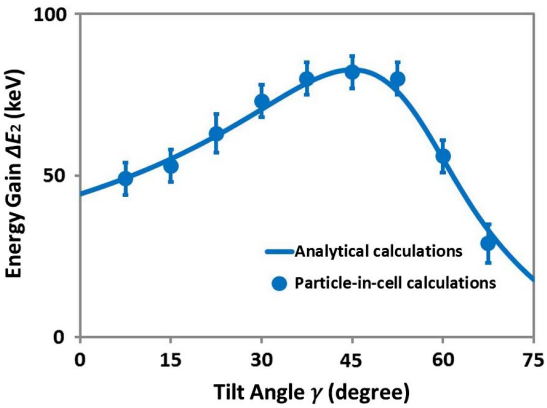

Fig. 6. Energy gain from analytical (blue line) and particle-in-cell (blue dots) calculations with different tilt angles, for a 100-period dual-grating structure: $E_0 = 3$ GV/m, $\tau_0 = 100$ fs, $L_{\text{int}} = 51$ μm. The error bars indicate the 68% confidence interval.

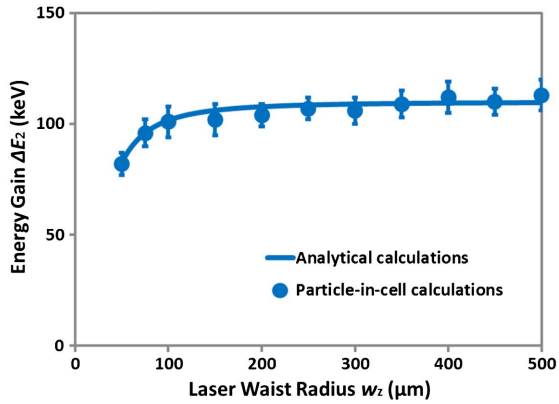

Fig. 7. Energy gain from analytical (blue line) and particle-in-cell (blue dots) calculations with increasing laser waist radius, for a 100-period dual-grating structure: $E_0 = 3$ GV/m, $\tau_0 = 100$ fs, $\gamma = 45°$. The error bars indicate the 68% confidence interval.

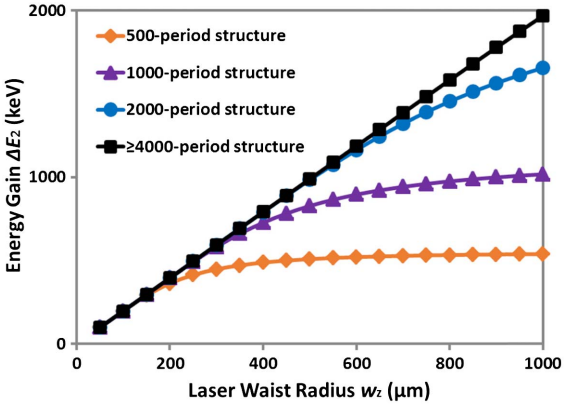

Fig. 8. Analytically calculated energy gain with increasing laser waist radius, for different periods of the dual-grating structure: $E_0 = 3$ GV/m, $\tau_0 = 100$ fs, $\gamma = 45°$.

For a dual-grating structure with over 4000 periods, corresponding to a length of $LZ = 4000$ μm, the energy gain increases linearly with the laser waist radius from 50 to 1000 μm. A laser waist radius of 1000 μm would generate an interaction length of $L_{\text{int}} = 1020$ μm from Eq. (15) and hence a maximum energy gain of 2.0 MeV, as shown in Fig. 8. This means that the energy gain can be greatly enhanced by PFT laser illumination, and that it depends strongly on the tilt angle, incident laser waist radius, and the number of structure periods.

5. CONCLUSION

This paper presented results from numerical studies into dual-grating DLAs driven by a PFT laser using the VSim simulation code. It was shown that this setup can extend the interaction length between laser and beam, thereby boosting the energy gain as compared to conventionally driven DLAs. Analytical studies to calculate the energy gain for normally incident and PFT lasers are also presented in this paper. For DLAs driven by a laser with a FWHM duration $\tau \leq 100$ fs, PFT laser

illumination generates a greater interaction length than a normal one. For longer FWHMs of $\tau > 100$ fs, there is a critical waist radius w_c, at which both schemes have the same interaction length, but when $w_z - w_c$, a PFT laser is more efficient than a normal one. We have also studied a dedicated optical system to generate our desired PFT laser beam with an ultrashort pulse duration of 100 fs, based on mathematical calculations. In order to have the maximum diffraction efficiency, a groove density of $n_g = 900$ lines/mm is chosen as optimum for our optical system. In this case, detailed investigations into electron beam acceleration and transmission for a laser waist radius of $w_z = 50$ μm are also presented. It has been found that the maximum gradient remains unchanged, but that the energy gain is increased by (91 ± 25) % for PFT laser illumination as compared to normal illumination. Moreover, it is also found that the energy gain is strongly dependent on the tilt angle, incident laser waist radius, and the number of structure periods. The maximum energy gain occurs at a tilt angle of 45° for relativistic electrons. For a 100-period dual grating, when the incident laser waist radius w_z increases from 50 to 500 μm, the energy gain gradually saturates to 110 ± 7 keV. For an incident laser with a waist radius of 1000 μm, a PFT laser beam with an interaction length of $L_{int} = 1020$ μm can be generated using our optical system. When such a PFT laser beam is introduced to illuminate a dual-grating structure with over 4000 periods, a maximum energy gain of 2.0 MeV can be expected.

By using such an optical system, we can generate the desired PFT laser beam to extend the interaction length, and so boost the energy gain for any DLA structure. However, further experimental studies on DLAs driven by a PFT laser beam are needed to verify the numerical calculations in this paper.

Funding. FP7 People: Marie-Curie Actions (PEOPLE) (289191); Science and Technology Facilities Council (STFC) (ST/G008248/1).

Acknowledgment. We thank Dr. Steven Jamison for many useful discussions.

REFERENCES

1. T. Plettner, P. P. Lu, and R. L. Byer, "Proposed few-optical cycle laser-driven particle accelerator structure," Phys. Rev. ST Accel. Beams **9**, 111301 (2006).
2. X. E. Lin, "Photonic band gap fiber accelerator," Phys. Rev. ST Accel. Beams **4**, 051301 (2001).
3. B. M. Cowan, "Three-dimensional dielectric photonic crystal structures for laser-driven acceleration," Phys. Rev. ST Accel. Beams **11**, 011301 (2008).
4. B. Naranjo, A. Valloni, S. Putterman, and J. B. Rosenzweig, "Stable charged-particle acceleration and focusing in a laser accelerator using spatial harmonics," Phys. Rev. Lett. **109**, 164803 (2012).
5. E. A. Peralta, K. Soong, R. J. England, E. R. Colby, Z. Wu, B. Montazeri, C. McGuinness, J. McNeur, K. J. Leedle, D. Walz, E. B. Sozer, B. Cowan, B. Schwartz, G. Travish, and R. L. Byer, "Demonstration of electron acceleration in a laser-driven dielectric microstructure," Nature **503**, 91–94 (2013).
6. K. P. Wootton, Z. Wu, B. M. Cowan, A. Hanuka, I. V. Makasyuk, E. A. Peralta, K. Soong, R. L. Byer, and R. J. England, "Demonstration of acceleration of relativistic electrons at a dielectric microstructure using femtosecond laser pulses," Opt. Lett. **41**, 2696–2699 (2016).
7. J. Breuer and P. Hommelhoff, "Laser-based acceleration of nonrelativistic electrons at a dielectric structure," Phys. Rev. Lett. **111**, 134803 (2013).
8. K. J. Leedle, R. F. Pease, R. L. Byer, and J. S. Harris, "Laser acceleration and deflection of 96.3 keV electrons with a silicon dielectric structure," Optica **2**, 158–161 (2015).
9. K. J. Leedle, A. Ceballos, H. Deng, O. Solgaard, R. F. Pease, R. L. Byer, and J. S. Harris, "Dielectric laser acceleration of sub-100 keV electrons with silicon dual-pillar grating structures," Opt. Lett. **40**, 4344–4347 (2015).
10. A. Aimidula, M. A. Bake, F. Wan, B. S. Xie, C. P. Welsch, G. Xia, O. Mete, M. Uesaka, Y. Matsumura, M. Yoshida, and K. Koyama, "Numerically optimized structures for dielectric asymmetric dual-grating laser accelerators," Phys. Plasmas **21**, 023110 (2014).
11. A. Aimidula, C. P. Welsch, G. Xia, K. Koyama, M. Uesaka, M. Yoshida, O. Mete, and Y. Matsumura, "Numerical investigations into a fiber laser based dielectric reverse dual-grating accelerator," Nucl. Instrum. Methods Phys. Res. Sect. A **740**, 108–113 (2014).
12. C. M. Chang and O. Solgaard, "Silicon buried gratings for dielectric laser electron accelerators," Appl. Phys. Lett. **104**, 184102 (2014).
13. Y. Wei, S. Jamison, G. Xia, K. Hanahoe, Y. Li, J. D. A. Smith, and C. P. Welsch, "Beam quality study for a grating-based dielectric laser-driven accelerator," Phys. Plasmas **24**, 023102 (2017).
14. J. Breuer, J. McNeur, and P. Hommelhoff, "Dielectric laser acceleration of electrons in the vicinity of single and double grating structures—theory and simulations," J. Phys. B **47**, 234004 (2014).
15. S. Akturk, X. Gu, E. Zeek, and R. Trebino, "Pulse-front tilt caused by spatial and temporal chirp," Opt. Express **12**, 4399–4410 (2004).
16. O. Martinez, "Pulse distortions in tilted pulse schemes for ultrashort pulses," Opt. Commun. **59**, 229–232 (1986).
17. M. E. Durst, G. Zhu, and C. Xu, "Simultaneous spatial and temporal focusing in nonlinear microscopy," Opt. Commun. **281**, 1796–1805 (2008).
18. J. A. Fülöp, L. Pálfalvi, G. Almási, and J. Hebling, "Design of high-energy terahertz sources based on optical rectification," Opt. Express **18**, 12311–12327 (2010).
19. VSim, available from https://www.txcorp.com/vsim.
20. J. A. Clarke, D. Angal-Kalinin, N. Bliss, R. Buckley, S. Buckley, R. Cash, P. Corlett, L. Cowie, G. Cox, G. P. Diakun, D. J. Dunning, B. D. Fell, A. Gallagher, P. Goudket, A. R. Goulden, D. M. P. Holland, S. P. Jamison, J. K. Jones, A. S. Kalinin, W. Liggins, L. Ma, K. B. Marinov, B. Martlew, P. A. McIntosh, J. W. McKenzie, K. J. Middleman, B. L. Militsyn, A. J. Moss, B. D. Muratori, M. D. Roper, R. Santer, Y. Saveliev, E. Snedden, R. J. Smith, S. L. Smith, M. Surman, T. Thakker, N. R. Thompson, R. Valizadeh, A. E. Wheelhouse, P. H. Williams, R. Bartolini, I. Martin, R. Barlow, A. Kolano, G. Burt, S. Chattopadhyay, D. Newton, A. Wolski, R. B. Appleby, H. L. Owen, M. Serluca, G. Xia, S. Boogert, A. Lyapin, L. Campbell, B. W. J. McNeil, and V. V. Paramonov, "CLARA conceptual design report," J. Instrum. **9**, T05001 (2014).
21. P. Piot, V. Shiltsev, S. Nagaitsev, M. Church, P. Garbincius, S. Henderson, and J. Leibfritz, "The advanced superconducting test accelerator (ASTA) at Fermilab: a user-driven facility dedicated to accelerator science & technology," arXiv:1304.0311 (2013).
22. C. Warner III and F. Rohrlich, "Energy loss and straggling of electrons," Phys. Rev. **93**, 406–407 (1954).